UKPMC Funders Group Author Manuscript

[14]Cell Signaling & Apoptosis Group at CIBERNED and Vall d'Hebron Institut of Research (VHIR) and Dept Biochemistry-molecular Biology and Institut de Neurociencies at Universitat Autonoma de Barcelona, Barcelona, Spain

[15]Heart Science Centre, National Heart and Lung Institute, Imperial College London, Harefield Hospital, Harefield, Middlesex, UB9 6JH, UK

[16]Cardiovascular Biomedical Research Unit, Royal Brompton and Harefield NHS Trust, Sydney Street, London, SW3 6NP

[17]Department of Epidemiology and Biostatistics, Faculty of Medicine, Imperial College London, Praed Street, London W2 1PG, UK

Abstract

Left ventricular mass (LVM) is a highly heritable trait[1] and an independent risk factor for all-cause mortality[2]. To date, genome-wide association studies (GWASs) have not identified the genetic factors underlying LVM variation[3] and the regulatory mechanisms for blood pressure (BP)-independent cardiac hypertrophy remain poorly understood[4,5]. Unbiased systems-genetics approaches in the rat[6,7] now provide a powerful complementary tool to GWAS and we applied integrative genomics to dissect a highly replicated, BP-independent LVM locus on rat chromosome 3p. We identified endonuclease G (*Endog*), previously implicated in apoptosis[8] but not hypertrophy, as the gene at the locus and demonstrated loss-of-function mutation in *Endog* associated with increased LVM and impaired cardiac function. Inhibition of *Endog* in cultured cardiomyocytes resulted in an increase in cell size and hypertrophic biomarkers in the absence of pro-hypertrophic stimulation. Genome-wide network analysis unexpectedly inferred *ENDOG* in fundamental mitochondrial processes unrelated to apoptosis. We showed direct regulation of *ENDOG* by *ERRα* and *PGC1α*, master regulators of mitochondrial and cardiac function[9,10,11], interaction of ENDOG with the mitochondrial genome and *ENDOG*-mediated regulation of mitochondrial mass. At baseline, *Endog* deleted mouse heart had depleted mitochondria, mitochondrial dysfunction and elevated reactive oxygen species (ROS), which was associated with enlarged and steatotic cardiomyocytes. Our studies establish further the link between mitochondrial dysfunction, ROS and heart disease and demonstrate a new role for *Endog* in maladaptive cardiac hypertrophy.

Elevated left ventricular mass (LVM) is a clinically important trait that independently predicts the risk of heart failure, sudden death and all-cause mortality[2]. Although LVM is a heritable complex trait[1], large genome wide association studies (GWASs) have not identified new LVM genes[3]. Blood pressure (BP)-dependent regulation of LVM, which is perhaps surprisingly limited[7], has been studied extensively in model systems and acts through well-characterised and overlapping signalling modules[12]. In contrast, the pathways underlying BP-independent cardiac hypertrophy, commonly seen in obesity and type 2 diabetes and related to mitochondrial dysfunction and liptoxicity[4,5], remain largely unknown. Here, we took advantage of the recent step-changes in integrative systems-genetics approaches in the rat[6,7] to dissect a BP-independent cardiac mass quantitative trait locus (QTL) and identified the causative gene and underlying mechanism.

The rat is unique for the study of cardiac mass with over 75 QTLs identified for this trait (rat genome database; http://rgd.mcw.edu/). Rat chromosome 3p (0-25Mbp) contains a highly replicated and BP-independent QTL for cardiac mass, which was mapped in crosses of the Spontaneously Hypertensive Rat (SHR) or SHR Stoke Prone (SHRSP) to Wistar Kyoto (WKY) or Salt Sensitive (SS)[13,14]. To dissect genetically this locus, we generated an F_2 intercross from SHR and Brown Norway (BN) strains and replicated further the LVM QTL (LOD=4.2) (Fig. 1a). We confirmed the BP-independent QTL effect in a congenic strain

(SHR.BN-(3L)) that had lower LVM and smaller cardiomyocytes than the SHR (Fig. 1b,c) and refined the QTL region (6.4Mbp-11.2Mpb) using a second congenic strain (SHR.BN-(3S)) (Supplementary Fig. 1). In the F_2 cross, in the SHR.BN-(3L) strain and in previous experimental crosses[13,14], the SHR allele at the locus was associated with increased cardiac mass and this effect was BP-independent (Fig. 1a and d). Functional assessment *in vivo* revealed that the SHR.BN-(3L) strain had better cardiac performance at baseline and following stimulation, as compared to the SHR (Supplementary Fig. 1). These data demonstrate that an SHR allele at the cardiac mass QTL on rat chromosome 3p increases LVM and adversely affects cardiac function.

We used the new genotypes generated in our F_2 cross and those from previous experiments[13,14] to refine the QTL region, and identified five distinct loci (spanning 750kbp in total) that co-segregated with the haplotypes associated with LVM variation (Fig. 1e). *Endonuclease G* (*Endog*), which we had previously shown to be *cis*-regulated in the heart ($P=3\times10^{-6}$)[7], was the only gene at the loci to be differentially regulated with consistent direction of effect in the SHR and SHRSP heart as compared to the WKY heart (Supplementary Table 1). *Endog* is a nuclear-encoded, mitochondrial-localised nuclease with a proposed but disputed function in apoptosis[8,15,16,17] and no known effect on cardiac mass or function. We observed reduced expression of *Endog* transcript and lack of Endog protein in all strains with elevated cardiac mass (Fig. 1f and g). Sequencing of *Endog* revealed promoter and coding sequence variation and we identified an SHR-specific, frameshift-causing insertion in *Endog* exon one that was associated with increased heart weight and LVM (Supplementary Fig. 2). There was marked reduction in cardiac nuclease activity, which was Endog-dependent[18], in SHR heart as compared to BN heart (Fig. 1h and i). In recombinant inbred strains derived from the SHR and BN[6,7] we confirmed the direct relationship between the SHR insertion and the lack of nuclease activity (Fig. 1j) and mapped *Endog*-dependent nuclease activity to a single locus that encodes *Endog* (Fig. 1k) . These data identify *Endog* as the candidate gene at the QTL and infer *Endog* loss-of-function as the mechanism for increased cardiac mass and impaired heart function.

We performed immunoblotting across rat and mouse tissues and determined that Endog was most highly expressed in the heart, localised to cardiomyocytes (Fig. 2) and co-localised with mitochondria (Supplementary Fig. 3). Using short hairpin RNA (shRNA) knockdown of *Endog* (sh*Endog*)[19] we tested the effect of *Endog* loss-of-function in cardiomyocytes and observed an increase in hypertrophic biomarkers and cell size in the absence of pro-hypertrophic stimulation (Fig. 2). Conventional BP-dependent hypertrophic signalling pathways[12] were not activated in sh*Endog* treated cells but we established activation of AMPK (Supplementary Fig. 4), which can induce cardiac hypertrophy[20]. We also observed increased reactive oxygen species (ROS), an additional pro-hypertrophic stimulus[21] that acts through multiple downstream effectors (Supplementary Fig. 4). These data show that *Endog* loss-of-function directly induces cardiac myocyte hypertrophy *in vitro* that is associated with the activation of two pro-hypertrophic pathways both of which have previously been linked with mitochondrial dysfunction[20,21,22].

We then examined the effects of *Endog* loss-of-function *in vivo* in the *Endog* deleted mouse (*Endog*$^{-/-}$)[17] that exhibits no detectable variation in apoptotic phenotypes, an observation that was confirmed in an independent *Endog* deleted strain[16]. As compared to controls, *Endog*$^{-/-}$ mice had larger cardiomyocytes at baseline (Fig. 2) in the absence of stimulation, in keeping with our observations in the SHR.BN-(3L) rat (Fig. 1) and *in vitro* (Fig. 2). Following angiotensin II stimulation of hypertrophy, which is largely ROS-dependent[21], we observed an increase in cardiomyocyte size, hypertrophic biomarkers and LVM in *Endog*$^{-/-}$ mice (Fig. 2 and Supplementary Fig 5). *Endog*$^{-/-}$ mice had BPs equivalent to control mice at baseline ($P=0.49$) and following angiotensin II stimulation ($P=0.51$). Our combined *in vitro*

UKPMC Funders Group Author Manuscript

and *in vivo* data confirm a role for *Endog* in cardiomyocyte hypertrophy and identify ROS as a conserved pro-hypertrophic stimulus in both systems.

Endog was proposed[8] but subsequently disputed[16,17] as important for apoptotic cell death and it was unclear how *Endog* loss-of-function was associated with cardiac hypertrophy and dysfunction. To infer *ENDOG* function in the human heart, we carried out genome-wide coexpression network analysis[23] in a large human cardiac expression dataset (n=210) (Supplementary Methods). *ENDOG* was identified in a network that was highly enriched for mitochondrial genes ($P=1.8\times10^{-58}$) and oxidative metabolism processes ($P=4.7\times10^{-38}$) (Fig. 3) (Supplementary Tables 2 and 3). Taken together, the high levels of Endog expression in metabolically active organs (Fig. 2) and in brown fat (Supplementary Fig. 6), the unique co-expression of *ENDOG* with oxidative metabolism genes and the link with AMPK signalling and ROS production pointed to an unappreciated effect of *Endog* in physiological mitochondrial processes.

Peroxisome proliferator activated receptor gamma coactivator 1 alpha (*Pgc1α*) is widely recognised as a master regulator of mitochondrial function[24], and activates many target genes component of the *ENDOG*-associated network (Fig. 3) through interaction with estrogen-related receptor alpha (*Errα*)[9]. Therefore, we tested whether *Pgc1α* also regulated *Endog* and observed robust *Pgc1α*-induced *Endog* transcript and Endog protein expression in cardiomyocytes *in vitro* (Fig. 3). We confirmed the effects of *Pgc1α* variation on Endog protein expression *in vivo* using mice over-expressing *Pgc1α* under the control of muscle creatine kinase (MCK-*Pgc1α*) and in cardiac-specific *Pgc1α* deleted mice ($Pgc1\alpha^{\Delta C/\Delta C}$) (Fig. 3, Supplementary Methods). Luciferase studies revealed strong activation of the *Endog* promoter by *Pgc1α* and *Errα* together (Fig. 3e) and we confirmed direct binding of *ESRRα* to the *ENDOG* promoter by chromatin immuno-precipitation and PCR (ChIP-PCR) in a region containing an *ERRα* response element ($P<0.001$) (Fig. 3f). These data show that *Endog* is a direct target of *ESRRα* and *Pgc1α*, master regulators of mitochondrial and heart function, further inferring a role for *Endog* in mitochondrial and cardiac biology.

It was apparent that the effects of *Endog* loss-of-function on cardiac hypertrophy might be mediated through perturbation of mitochondrial physiology, which we examined. Electron microscopy revealed no gross morphological changes of mitochondria but we observed lipid-like droplets associated with mitochondria from $Endog^{-/-}$ mice that were more numerous and larger than those seen in control mice. Molecular studies revealed marked elevation of triglyceride levels in the $Endog^{-/-}$ mouse heart that was manifest as cardiomyocyte steatosis (Fig. 4 and Supplementary Fig. 7) but not associated with variation in expression levels of fatty acid metabolism or mitochondrial biogenesis genes (Supplementary Fig. 8 and 9). As compared to wildtype littermates, $Endog^{-/-}$ mice had impaired mitochondrial respiration and increased ROS production (Fig. 4).

To assess for mitochondrial depletion we examined mitochondrial DNA (mtDNA)/genomic DNA and mitochondrial protein/tissue weight ratios, which were both diminished in the $Endog^{-/-}$ mouse heart (Fig. 4) in the absence of mtDNA structural variation (Supplementary Fig. 10). This was an intriguing finding given the previously proposed roles for *Endog* in mtDNA synthesis, processing of poly-cistronic mtRNA and mitochondrial biogenesis[25,26] that were subsequently discarded based primarily on experiments in *Endog* deleted mice[16,17]. We re-examined a role of *ENDOG* in mitochondrial biogenesis and demonstrated an increase in mitochondrial mass with chronic *ENDOG* expression in HEK cells ($P<0.01$)and acute *Endog* over-expression in a cardiomyocyte-derived cell line ($P<0.001$) (Fig. 4k-k in the absence of an effect on apoptotic or necrotic cell death (Supplementary Fig. 11). A role for *ENDOG* in mtDNA biology[25,26] was supported further by ChIP-PCR experiments that showed direct binding of ENDOG throughout the mtDNA molecule (Fig.

UKPMC Funders Group Author Manuscript

4n) as previously demonstrated for mitochondrial transcription factor A (TFAM)[27], which is a critical determinant of mtDNA synthesis and repair that when deleted causes eccentric cardiac hypertrophy and heart failure[28].

Mitochondria are essential for oxidative metabolism and mitochondrial dysfunction/ depletion in the heart causes maladaptive cardiac hypertrophy and cardiac dysfunction associated with increased ROS and lipotoxicity[4,5,28,29]. Here we identified *Endog* loss-of-function as a primary determinant of maladaptive cardiac hypertrophy that was associated with mitochondrial dysfunction/depletion and marked cardiomyocyte steatosis. Although the mechanism underlying cardiac hypertrophy due to impaired mitochondrial function is not limited to a single pathway we demonstrated a conserved increase in ROS, an established hypertrophic stimulus[21,22], in *Endog* loss-of-function models. Our studies resolve some of the uncertainty as to the non-apoptotic function of *Endog*[15,16,17] and reveal it's importance in mitochondrial biology, which has intriguing parallels with the dual roles of apoptosis-inducing-factor[30]. We propose that *ENDOG*, which we show binds to mtDNA, modulates mtDNA synthesis, maintenance and/or transcription, in keeping with previous hypotheses[25,26]. Therapeutic targeting the *Pgc1α/Errα* axis has been proposed to improve mitochondrial function in cardiac failure[11] and our studies suggest that regulation of *Endog* is an important component of this process. We conclude that *Endog* is a novel determinant of maladaptive cardiac hypertrophy with previously unappreciated mitochondrial functions.

Methods Summary

Linkage mapping was carried out using microsatellite genotypes in the BNxSHR F_2 population. *Ex vivo* heart weight analysis was performed in the congenic strains, which were characterised using *in vivo* BP telemetry. Comparative haplotype analysis was performed using SNP data (Rat Genome Database; http://rgd.mcw.edu/) for all strains used in the QTL mapping studies. Microarray-based expression analysis was conducted as previously described[6,7]. Cell size and hypertrophy biomarker expression were measured in cardiomyocytes following lentivirus-mediated *Endog* knockdown. Heart weight, hypertrophic biomarker expression and cardiomyocyte cell size were measured in *Endog*$^{-/-}$ mice at baseline and following angiotensin II-induced hypertrophy. Triglyceride abundance, mitochondrial mass and respiratory activity were measured in *Endog*$^{-/-}$ mice as described in the Supplementary material. Weighted gene co-expression network analysis (WGCNA)[23] was applied to the largest publicly available human heart transcriptome dataset. Regulation of *Endog* by *Pgc1α* was investigated in Ad.*Pgc1α*-infected neonatal cardiomyocytes, MCK-*Pgc1* skeletal muscle and *Pgc1* $\alpha^{\Delta C/\Delta C}$ heart samples. ERRα association with the *ENDOG* promoter and *ENDOG*-mtDNA interaction were determined using ChIP. Histological analysis and electron microscopy of *Endog*$^{-/-}$ hearts was carried out to study mitochondrial structure and abundance as well as lipid deposition. MtDNA and gDNA copy number were assessed by QPCR. Mitochondrial abundance was studied in cells by flow cytometry. Full methods are provided in Supplementary Methods.

Supplementary Material

Refer to Web version on PubMed Central for supplementary material.

Acknowledgments

We acknowledge funding from the Medical Research Council (MRC) UK, the National Institute for Health Research (NIHR) UK, the Royal Brompton and Harefield Cardiovascular Biomedical Research Unit, the Imperial College Healthcare Biomedical Research Centre, the British Heart Foundation, the Fondation Leducq, the Wellcome Trust, 301/08/0166 from the Grant Agency of the Czech Republic and 1M0520 from the Ministry of Education of the Czech Republic, PTQ-08-03-07880, SAF2008-02271, SAF2008-03067 and SAF2010-19125 from

UKPMC Funders Group Author Manuscript

the Ministerio de Ciencia e Innovacion (MICINN, Spain), 2009-SGR-346 from the Agència de Gestió d'Ajuts Universitaris i Recerca (AGAUR, Spain), PS09/02034, PS09/01602 and PS09/01591 from Fondo de Investigaciones (FIS, Spain). The European Community's Seventh Framework Programme (FP7/2007-2013) under grant agreement no. HEALTH-F4-2010-241504 (EURATRANS). The German National Genome Research Network (NGFN-Plus) Heart Failure. We thank Dr Michael R. Lieber (University of Southern California) for providing the *Endog* deleted mice and Prof E. Wahle (Institute of Biochemistry and Biotechnology, Halle) for providing the CG4930 expression plasmid. We thank the National BioResource Project-Rat (http://www.anim.med.kyoto-u.ac.jp/NBR/) for providing rat strains.

References

1. Post WS, Larson MG, Myers RH, Galderisi M, Levy D. Heritability of left ventricular mass: the Framingham Heart Study. Hypertension. 1997; 30:1025–1028. [PubMed: 9369250]
2. Lorell BH, Carabello BA. Left ventricular hypertrophy: pathogenesis, detection, and prognosis. Circulation. 2000; 102:470–479. [PubMed: 10908222]
3. Vasan RS, et al. Genetic variants associated with cardiac structure and function: a meta-analysis and replication of genome-wide association data. JAMA. 2009; 302:168–178. [PubMed: 19584346]
4. McGavock JM, Victor RG, Unger RH, Szczepaniak LS. Adiposity of the heart, revisited. Ann Intern Med. 2006; 144:517–524. [PubMed: 16585666]
5. Wong C, Marwick TH. Obesity cardiomyopathy: pathogenesis and pathophysiology. Nat Clin Pract Cardiovasc Med. 2007; 4:436–443. [PubMed: 17653116]
6. Heinig M, et al. A trans-acting locus regulates an anti-viral expression network and type 1 diabetes risk. Nature. 2010; 467:460–464. [PubMed: 20827270]
7. Petretto E, et al. Integrated genomic approaches implicate osteoglycin (Ogn) in the regulation of left ventricular mass. Nat Genet. 2008; 40:546–552. [PubMed: 18443592]
8. Li LY, Luo X, Wang X. Endonuclease G is an apoptotic DNase when released from mitochondria. Nature. 2001; 412:95–99. [PubMed: 11452314]
9. Dufour CR, et al. Genome-wide orchestration of cardiac functions by the orphan nuclear receptors ERRalpha and gamma. Cell Metab. 2007; 5:345–356. [PubMed: 17488637]
10. Wu Z, et al. Mechanisms controlling mitochondrial biogenesis and respiration through the thermogenic coactivator PGC-1. Cell. 1999; 98:115–124. [PubMed: 10412986]
11. Finck BN, Kelly DP. PGC-1 coactivators: inducible regulators of energy metabolism in health and disease. J Clin Invest. 2006; 116:615–622. [PubMed: 16511594]
12. Hill JA, Olson EN. Cardiac plasticity. N Engl J Med. 2008; 358:1370–1380. [PubMed: 18367740]
13. Inomata H, et al. Identification of quantitative trait loci for cardiac hypertrophy in two different strains of the spontaneously hypertensive rat. Hypertens Res. 2005; 28:273–281. [PubMed: 16097372]
14. Siegel AK, et al. Genetic loci contribute to the progression of vascular and cardiac hypertrophy in salt-sensitive spontaneous hypertension. Arterioscler Thromb Vasc Biol. 2003; 23:1211–1217. [PubMed: 12775577]
15. Buttner S, et al. Endonuclease G regulates budding yeast life and death. Mol Cell. 2007; 25:233–246. [PubMed: 17244531]
16. David KK, Sasaki M, Yu SW, Dawson TM, Dawson VL. EndoG is dispensable in embryogenesis and apoptosis. Cell Death Differ. 2006; 13:1147–1155. [PubMed: 16239930]
17. Irvine RA, et al. Generation and characterization of endonuclease G null mice. Mol Cell Biol. 2005; 25:294–302. [PubMed: 15601850]
18. Temme C, et al. The Drosophila melanogaster Gene cg4930 Encodes a High Affinity Inhibitor for Endonuclease G. J Biol Chem. 2009; 284:8337–8348. [PubMed: 19129189]
19. Bahi N, et al. Switch from caspase-dependent to caspase-independent death during heart development: essential role of endonuclease G in ischemia-induced DNA proces sing of differentiated cardiomyocytes. J Biol Chem. 2006; 281:22943–22952. [PubMed: 16754658]
20. Arad M, et al. Constitutively active AMP kinase mutations cause glycogen storage disease mimicking hypertrophic cardiomyopathy. J Clin Invest. 2002; 109:357–362. [PubMed: 11827995]

21. Dai DF, et al. Mitochondrial oxidative stress mediates angiotensin II-induced cardiac hypertrophy and Galphaq overexpression-induced heart failure. Circ Res. 2011; 108:837–846. [PubMed: 21311045]
22. Seddon M, Looi YH, Shah AM. Oxidative stress and redox signalling in cardiac hypertrophy and heart failure. Heart. 2007; 93:903–907. [PubMed: 16670100]
23. Zhang B, Horvath S. A general framework for weighted gene co-expression network analysis. Stat Appl Genet Mol Biol. 2005; 4 Article17.
24. Spiegelman BM. Transcriptional control of mitochondrial energy metabolism through the PGC1 coactivators. Novartis Found Symp. 2007; 287:60–63. discussion 63-69. [PubMed: 18074631]
25. Cote J, Ruiz-Carrillo A. Primers for mitochondrial DNA replication generated by endonuclease G. Science. 1993; 261:765–769. [PubMed: 7688144]
26. Tiranti V, et al. Chromosomal localization of mitochondrial transcription factor A (TCF6), single-stranded DNA-binding protein (SSBP), and endonuclease G (ENDOG), three human housekeeping genes involved in mitochondrial biogenesis. Genomics. 1995; 25:559–564. [PubMed: 7789991]
27. Rothfuss O, et al. Parkin protects mitochondrial genome integrity and supports mitochondrial DNA repair. Hum Mol Genet. 2009; 18:3832–3850. [PubMed: 19617636]
28. Wang J, et al. Dilated cardiomyopathy and atrioventricular conduction blocks induced by heart-specific inactivation of mitochondrial DNA gene expression. Nat Genet. 1999; 21:133–137. [PubMed: 9916807]
29. Lewis W, et al. Decreased mtDNA, oxidative stress, cardiomyopathy, and death from transgenic cardiac targeted human mutant polymerase gamma. Lab Invest. 2007; 87:326–335. [PubMed: 17310215]
30. Vahsen N, et al. AIF deficiency compromises oxidative phosphorylation. EMBO J. 2004; 23:4679–4689. [PubMed: 15526035]

UKPMC Funders Group Author Manuscript

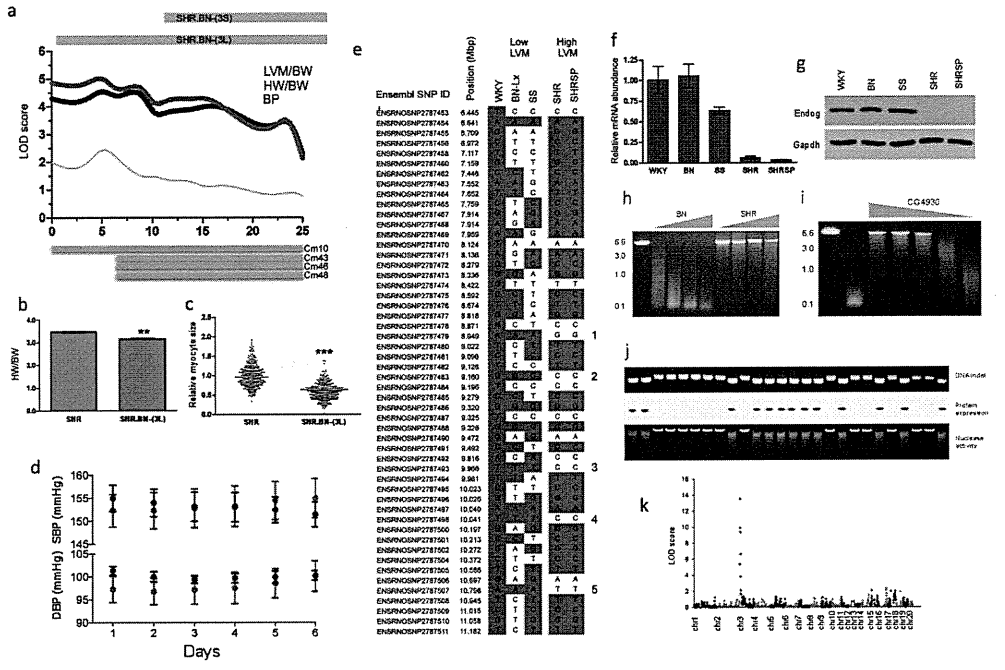

Figure 1. Positional cloning of *Endog* as the gene underlying the rat chromosome 3p cardiac mass quantitative trait locus (QTL)

a, Mapping of heart weight (HW) and left ventricular mass (LVM) corrected for body weight (BW) to chromosome 3p in the Brown Norway (BN) x Spontaneously Hypertensive (SHR) F_2 population. The telomeric limits of the congenic strains (SHR.BN-(3L) and SHR.BN-(3S)) and the previously mapped cardiac mass (CM) QTLs[13,14] are shown; x-axis, physical position in Mbp. **b**, HW indexed to BW in the SHR (n=4) and the SHR.BN-(3L) congenic strains (n=5). **c**, Relative cardiomyocyte cross-sectional area in SHR and SHR.BN-(3L) congenic strains. **d**, *In vivo* telemetric systolic- and diastolic-blood pressure (SBP and DBP) measurements in the SHR (red circles) and SHR.BN-(3L) (black circles) (n=8 per genotype). **e,** Haplotype analysis of the refined QTL region. SNPs are depicted with reference to WKY/NCrl alleles (grey, identical; white, dissimilar) with numbers (1-5) denoting the polymorphic regions between strains with either high or low HW. QPCR of *Endog* mRNA expression (**f**) and immunoblot of Endog protein expression (**g**) in strains with low or high CM at the chromosome 3p locus. **h,** Nuclease activity in BN and SHR heart extracts over a range of cardiac protein extract amounts (grey wedge) (Supplementary Methods). **i**, Reversal of nuclease activity in cardiac lysates by a drosophila-derived inhibitor of Endog[18] (range 1500nM-1.5nM, grey wedge). **j**, Association of the *Endog* indel with loss of Endog protein expression and diminished nuclease activity in the recombinant inbred (RI) strains. Upper, middle and lower panels display the DNA indel, protein expression and nuclease activity, respectively. **k**, Linkage mapping of nuclease activity in RI strains using a quantitative fluorescence-based assay (Supplementary Methods). All data are represented as mean+s.e.m. *, $P<0.05$, **, $P<0.01$, ***, $P<0.001$.

UKPMC Funders Group Author Manuscript

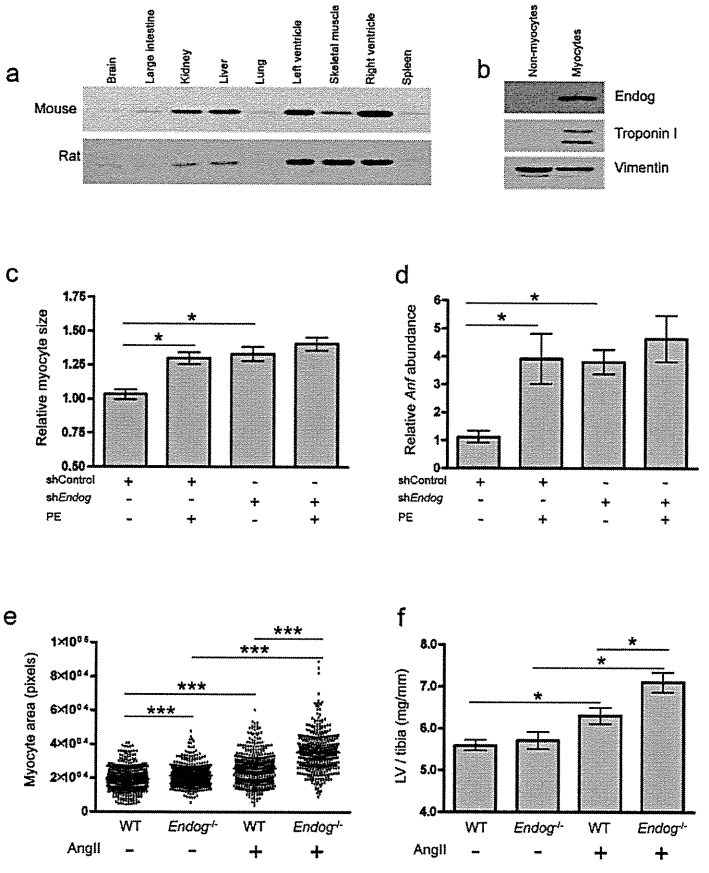

Figure 2. *Endog* regulates cardiac hypertrophy

a, Immunoblot of Endog expression in mouse and rat tissues (Endog: ~30 kDa). **b**, Immunoblot of Endog expression in myocyte and non-myocyte populations isolated from neonatal rat heart. **c**, Cardiomyocyte size (n≥100 cells, n=3 independent experiments) treated with shRNA against *Endog* (sh*Endog*) or control shRNA (shControl) in the presence or absence of the hypertrophic stimulant phenylephrine (PE, 100μM, 24 h). **d**, Expression of the hypertrophic biomarker *Anf* in sh*Endog* and shControl treated cells. **e**, Cardiomyocyte size (Supplementary Fig. 5) in *Endog*$^{-/-}$ and wildtype (WT) mice at baseline and following angiotensin II-induced cardiac hypertrophy. **f**, LVM/tibial length in *Endog*$^{-/-}$ and WT mice at baseline and following AngII stimulation. Data are represented as mean+s.e.m. *, $P<0.05$, **, $P<0.01$, ***, $P<0.001$.

UKPMC Funders Group Author Manuscript

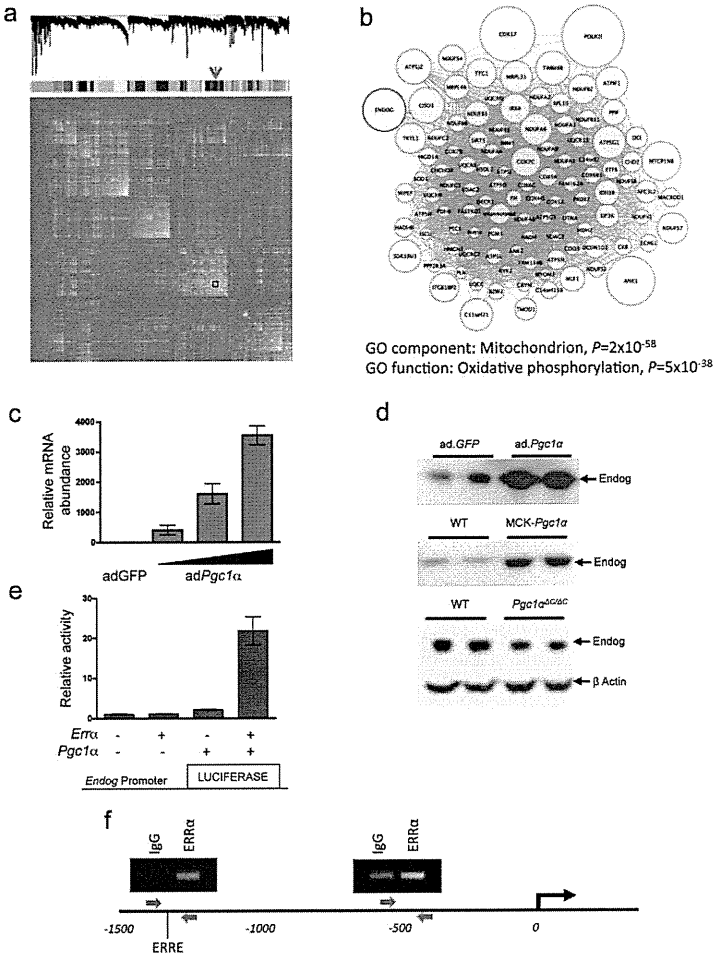

Figure 3. *ENDOG* is co-expressed with a mitochondrial-specific gene network and regulated by *Pgc1α* and *ERRα*

a, Genes (8,490 from 210 datasets) are clustered and plotted based on the dissimilarity metric between their expression profiles (Supplementary Methods). From top to bottom: low-hanging branches in the dendrogram represent groups of genes (modules) that have a high similarity metric. Modules are shown beneath the dendrogram and are colour coded. The arrow indicates the module (also boxed) containing *ENDOG*. In the heat-map of the correlations between expression profiles, high and low similarities are coloured yellow and red, respectively. **b**, Weighted gene co-expression network analysis (WGCNA[23]) for the module containing *ENDOG*, providing functional annotation by cellular localization by Gene Ontology classification (Supplementary Tables 2 and 3). Nodes represent genes and edges represent significant co-expression between genes. The node size is proportional to the relative degree of interconnectivity of each gene within the module. **c**, QPCR analysis of *Endog* expression in cultured cardiomyocytes following infection with adenovirus (ad) expressing *GFP* (ad.*GFP*) or *Pgc1α* (ad.*Pgc1α*). **d**, Immunoblot of Endog expression in ad.*Pgc1α*-infected cardiomyocytes (top panel), skeletal muscle of wild-type (WT) mice and transgenic mice expressing *Pgc1α* under the control of muscle creatine kinase (MCK-*Pgc1α*) (middle panel), and in hearts of WT and cardiac-specific *Pgc1α* deleted mice ($Pgc1\alpha^{\Delta C/\Delta C}$) (bottom panel). **e**, *Endog* promoter activity in HEK293 cells infected with ad.*Pgc1α* and and/or ad.*Errα*. **f**, ERRα chromatin immunoprecipitation (ChIP) and PCR of two regions of the *ENDOG* promoter. Red arrows denote primers and ERRE specifies the

location of a consensus ERR response element (1304 bases upstream). The experiment was repeated three times with similar results and PCR products quantified by QPCR.

UKPMC Funders Group Author Manuscript

UKPMC Funders Group Author Manuscript

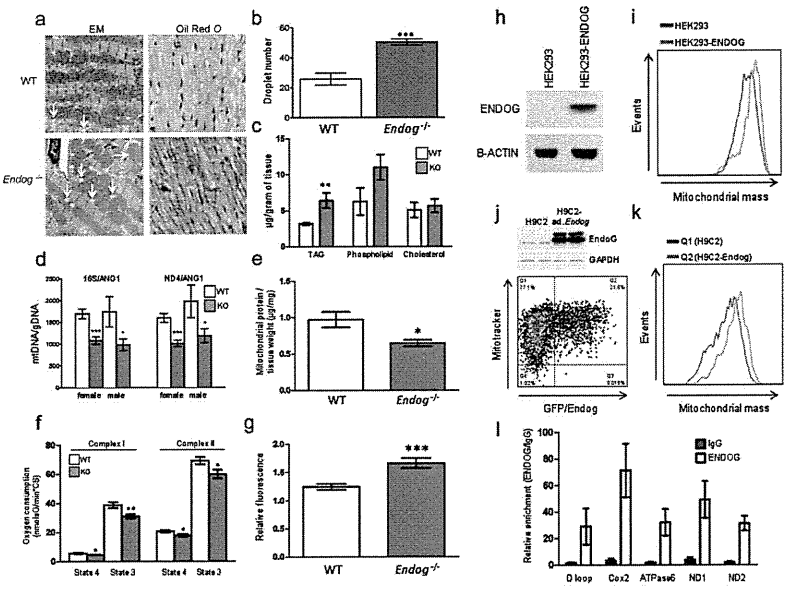

Figure 4. *Endog* regulates mitochondrial function and cardiac lipid metabolism

a, Transmission electron micrographs and oil red *O* stained micrographs (high resolution, Supplementary Fig. 7) of left ventricular sections from WT and *Endog*$^{-/-}$ mice. **b,** Quantification of the number of mitochondrial-associated droplets in WT and *Endog*$^{-/-}$ mice. **c**, Quantification of cardiac triglyceride (TAG), phospholipid and cholesterol content in WT and *Endog*$^{-/-}$ mice (n=5). **d**, Ratio of mitochondrial DNA (mtDNA) to genomic DNA (gDNA) in hearts of WT and *Endog*$^{-/-}$ mice. **e,** Quantification of mitochondrial protein content in WT and *Endog*$^{-/-}$ mice (n=5). **f**, State 3 and state 4 oxygen consumption in the presence of complex I or complex II substrates in isolated cardiac mitochondria from WT (n=6) and *Endog*$^{-/-}$ (n=5) mice. **g**, Relative fluorescence-based measurement of ROS production by mitochondria isolated from WT (n=6) and *Endog*$^{-/-}$ (n=5) mice. **h-k**, Representative flow cytometry analysis of mitochondrial mass in HEK293 and H9C2 cells over-expressing ENDOG or Endog, respectively (n=4). **h**, Stable expression of *ENDOG* in HEK293 cells (HEK293-*ENDOG*). **i,** Flow cytometry analysis of HEK293 and HEK293-*ENDOG* cells stained with mitotracker. **j,** Adenovirus (ad)-mediated expression of GFP and Endog in myocytes and flow cytometry analysis of ad.*Endog* infected cells (Q2) and uninfected control cells (Q1). **k**, Number of events plotted against mitochondrial mass in ad.*Endog* infected (Q2) and control (Q1) H9C2 cells. **l**, QPCR of mtDNA-protein complexes following ChIP of mitochondrial chromatin using anti-ENDOG antibody or IgG. All data are represented as mean+s.e.m. *, $P<0.05$, **, $P<0.01$, ***, $P<0.001$.

Kuramoto et al. BMC Genetics 2011, 12:91
http://www.biomedcentral.com/1471-2156/12/91

BMC Genetics

RESEARCH ARTICLE Open Access

A rat model of hypohidrotic ectodermal dysplasia carries a missense mutation in the *Edaradd* gene

Takashi Kuramoto*, Mayuko Yokoe, Ryoko Hashimoto, Hiroshi Hiai and Tadao Serikawa

Abstract

Background: Hypohidrotic ectodermal dysplasia (HED) is a congenital disorder characterized by sparse hair, oligodontia, and inability to sweat. It is caused by mutations in any of three Eda pathway genes: ectodysplasin (*Eda*), Eda receptor (*Edar*), and Edar-associated death domain (*Edaradd*), which encode ligand, receptor, and intracellular adaptor molecule, respectively. The Eda signaling pathway activates NF-κB, which is central to ectodermal differentiation. Although the causative genes and the molecular pathway affecting HED have been identified, no curative treatment for HED has been established. Previously, we found a rat spontaneous mutation that caused defects in hair follicles and named it sparse-and-wavy (*swh*). Here, we have established the *swh* rat as the first rat model of HED and successfully identified the *swh* mutation.

Results: The *swh/swh* rat showed sparse hair, abnormal morphology of teeth, and absence of sweat glands. The ectoderm-derived glands, meibomian, preputial, and tongue glands, were absent. We mapped the *swh* mutation to the most telomeric part of rat Chr 7 and found a Pro153Ser missense mutation in the *Edaradd* gene. This mutation was located in the death domain of EDARADD, which is crucial for signal transduction and resulted in failure to activate NF-κB.

Conclusions: These findings suggest that *swh* is a loss-of-function mutation in the rat *Edaradd* and indicate that the *swh/swh* rat would be an excellent animal model of HED that could be used to investigate the pathological basis of the disease and the development of new therapies.

Background

Hypohidrotic ectodermal dysplasia (HED) is a genetic disorder characterized by sparse hair, oligodontia, reduced sweating, and defects in a number of other ectodermal organs [1]. A lack of sweat glands can lead to recurrent severe overheating. Thus, children with HED are at substantial risk of sudden death in infancy due to fatal hyperpyrexia [2].

HED is caused by mutations in any of the three Eda pathway genes: ectodysplasin (*Eda*) [3,4], ED receptor (*Edar*) [5], and EDAR-associated death domain (*Edaradd*) [6]. They encode the ligand, receptor, and intracellular signal mediator of a single linear pathway, respectively. The Eda signaling pathway activates transcription factor NF-κB thereby playing an important role in embryonic development, especially in the development of ectodermally derived organs [1].

* Correspondence: tkuramot@anim.med.kyoto-u.ac.jp
Institute of Laboratory Animals, Graduate School of Medicine, Kyoto University, Yoshidakonoe-cho, Sakyo-ku, Kyoto 606-8501, Japan

In humans, there are three types of HED with different inheritance: X-linked HED, autosomal dominant HED, and autosomal recessive HED. X-linked HED is the most common form of HED and is caused by mutations in *EDA*. Autosomal HED is caused by mutations in *EDAR* or *EDARADD*. Currently, over 100 different mutations in the *EDA* gene are known, while only ~20 and 4 causative mutations have been found in *EDAR* and *EDARADD*, respectively [7].

To date, four mouse models of HED are available: *Tabby, downless, Sleek*, and *crinkled*. The mutant phenotype of the *Tabby* mouse is inherited in an X-linked manner and the *Tabby* mouse carries a mutation in the *Eda* gene [4]. The recessive *downless* and dominant *Sleek* mice carry mutations in the *Edar* gene [8]. The *crinkled* mouse carries a mutation in the *Edaradd* gene [6]. The phenotypes in *Eda, Edar*, and *Edaradd* mutant mice are almost identical and include abnormalities in teeth, hair, and sweat glands, the triad of symptoms of HED. Over 20 different glands, including lacrimal, meibomian, salivary,

submandibular, and mammary glands, are also affected [9-11]. These mutant mice have been used to study the roles of the Eda pathway in the development and morphogenesis of ectoderm-derived organs and to develop a novel treatment for HED using a recombinant EDA protein [12].

Mutations in some of the genes in the Eda pathway have been identified in various species, such as medaka [13], zebrafish [14], cattle [15-18], and dog [19]. Analyses of these mutations showed critical roles of the Eda pathway in the development of epithelial appendages, as well as in morphological evolution. Thus, the identification of novel mutations in different species emphasized the importance of the Eda pathway, and enabled the phenotypes of the mutated animals to be compared, giving new insights into the functions of the Eda pathway. If such novel mutations can be identified in mammals, then the affected species could be used as a disease model of HED.

In a previous study, we described a mutant rat, sparse and wavy hair (*swh*), which arose spontaneously in a colony of inbred WTC rats in 1998 [20]. The mutant phenotype is characterized by sparse and wavy hair, impaired body weight gain, and hypoplasticity of the mammary gland. The hair follicles in these rats were reduced both in number and size, a characteristic associated with hypoplasia of both the sebaceous glands and the subcutaneous fat tissues. The mammary glands of *swh/swh* female rats were hypoplastic and differentiation of mammary epithelial and myoepithelial cells was impaired. Thus, it is conceivable that the *swh/swh* rat will provide a good experimental model to clarify the mechanisms involved in the development of skin appendages, most of which are derived from ectoderm [20].

In our previously reported linkage analysis, *swh* mapped to the telomeric part of rat Chr 17. At that time, the physical location of the *swh* locus could not be accurately determined because a SSLP marker, *D17Rat140*, which defined the distal side of the *swh* locus was, in the earlier public rat genome linkage map, erroneously assigned to the middle part of Chr 17 and not to the telomeric part of Chr 17. Recently, with the development of more than 20,000 single nucleotide polymorphism (SNP) markers for 167 rat inbred strains and with the haplotype mapping data from the genotyping of these SNPs, the genome linkage map has been improved [21]. In the improved rat genome map, *D17Rat140* and its neighboring genes are correctly mapped to the telomeric part of rat Chr 17. Thus, in addition to the 24 candidate genes selected from our previous linkage analysis, we also considered these newly mapped genes to be candidates of *swh* [20].

In this study, to demonstrate the suitability of the *swh* rat as an HED model, we investigated the pathology of tissues and organs in which morphological abnormalities in HED are known to occur. Furthermore, we identified the causative mutation of the *swh* phenotype using a positional cloning approach, and found a missense mutation in the death domain of EDARADD, that might explain the inability of the mutant *Edaradd* gene to activate NF-κB. Our findings suggest that *swh* is a loss-of-function mutation of the rat *Edaradd* and support the *swh/swh* rat as an excellent animal model of HED that can be used to investigate the pathological basis of the disease and to develop new therapies.

Methods

Animals

ACI/NKyo, WTC/Kyo, and WTC-*swh*/Kyo rats were provided by the Japanese National BioResource Project for the Rat and kept in our animal facility for all experiments in this study. Animal care and experimental procedures were approved by the Animal Research Committee, Kyoto University, Japan, and were conducted according to the Regulation on Animal Experimentation at Kyoto University.

Histopathology

For light microscopy, the tongue, eyelid, ventral skin, footpad, and preputial gland were harvested from WTC-*swh/swh* and WTC rats at 8 weeks of age. Tissues were fixed in 10% neutral-buffered formalin, embedded in paraffin, and stained with hematoxylin and eosin (HE).

Sweat tests and whole mount staining of mammary glands

The sweat test was performed as described previously [12]. Briefly, the hind paws of rats anesthetized with sevoflurane were painted with a solution of 3% (wt/vol) iodine in ethanol. Once dry, the paws were painted with a suspension of 40% (wt/vol) starch I mineral oil. Photographs were taken 1 min later and sweat was detected as dark spots. Mammary glands were prepared as a whole mount and stained as described previously [22].

Fine mapping of swh

For fine mapping of *swh*, F2 animals (n = 769) were produced by intercrossing (ACI/NKyo × WTC-*swh*) F1 rats. Homozygous *swh/swh* animals were identified at 3-4 weeks of age based on the appearance of the sparse-and-waved hair phenotype. One hundred and ninety-eight *swh/swh* homozygotes were used for fine mapping of *swh*. Genomic DNA was prepared from tail biopsies using the automatic DNA purification system (PI-200; Kurabo, Japan).

RNA extraction, RT-PCR and direct sequencing

Total RNA was extracted from the skin of 2-week-old animals. RNA preparation, RT-PCR and direct sequencing of PCR products were performed as described

previously [23]. Rat *Edaradd* cDNAs were amplified with 6 sets of primers (Table 1). The PCR products overlapped each other and spanned the entire coding sequence of *Edaradd*.

Transient transfection and reporter assays

The NF-κB assay was designed to test for activation of the NF-κB responsive promoter. HEK293T cells grown in poly-L-lysine coated 24-well plates were transfected using SuperFect (Qiagen) with 1.2 μg pNF-κB-Luc (Clontech), 2 μg pRL-TK, and an increasing amount of expression vectors encoding the wild-type EDARADD or the *swh*-type EDARADD (Pro153Ser). The Luc reporter of the pNF-κB-Luc encodes firefly luciferase. The HSV-TK (herpes simplex virus thymidine kinase) promoter drives renilla luciferase in pRL-TK. Total DNA was adjusted to 2.6 μg by adding pCMV-HA (Clontech) vector as necessary. Luciferase activity was measured using the Dual-Luciferase Reporter Assay System (Promega) 48 h after transfection, according to the manufacturer's protocol.

Results

Phenotypes of *swh/swh* rat as hypohidrotic ectodermal dysplasia (HED)

Patients with HED display defective development of hair, teeth, sweat glands, and several exocrine glands, such as sebaceous, salivary, meibomian, and lacrimal [1,24]. To evaluate the relevance of the *swh/swh* rat as a HED model, we looked for developmental defects in those tissues of *swh/swh* rats. In addition to defects of the hair, skin, and mammary glands, which have been reported previously [20] (Figure 1A, B), we found defects in the sweat, meibomian, preputial, and tongue glands. In these tissues, the exocrine glands were absent in the *swh/swh* rats (Figure 1C, D, E, F). In the sweat test, no sweat was detected in *swh/swh* rats, indicating that the sweat glands were functionally defective (Figure 1C). We also found a reduced number of cusps in the lower first molars in the *swh/swh* rats (Figure 1G).

In the Eda pathway mutant mice, *Tabby, downless,* and *crinkled,* a kinked tail tip, a bald patch behind the ear, and abnormal pelage hair composition are characteristic. Similarly, in *swh/swh* rat, the pelage hair was composed of only an abnormal awl hair (Figure 1A); however, the tail had hair on it, the frequency of kinked tail was low, and the bald patch behind the ear was not found (Figure 1G).

These findings indicate that the mutant phenotypes of *swh/swh* rats are similar to developmental defects in HED patients and in the established mouse models; therefore, it is likely that the *swh/swh* rat will be suitable as a model of HED.

Positional cloning of *swh*

In a previous study, we mapped *swh* to rat Chr 17 [20]. To more specifically map the position of the *swh* locus, we genotyped F2 intercross progeny for markers known to be closely linked to *swh*. There was only one recombinant chromosome between *swh* and either *D17Rat132* or *D17Rat140* in 396 meioses (= 198 × 2) and we were able to map *swh* to the most distal part of Chr17 (Figure 2A). The rat genome map (RGSC v3.4) showed two genes in the *swh* locus, *Ero1lb* (ERO1-like beta (*S. cerevisiae*)) and *Edaradd* (ectodysplasin-A receptor-associated death domain). The mouse mutant of *Edaradd* is called *crinkled* (*cr*) and mice that carry this mutation show a sparse hair phenotype that is similar to that of the *swh* rat [25]. Additionally, mutations in the human *EDARADD* gene have been found in families affected with HED [6,26]. Thus, we considered *Edaradd* as a good candidate of *swh*. Although the abnormal expression of *Edaradd* mRNA was not detected in the skin of *swh/swh* rats (data not shown), we found a missense mutation (C to T) in exon 6 of the *swh/swh Edaradd* gene. This mutation was deduced to change proline to serine at the 153rd amino acid (Pro153Ser) of the rat EDARADD protein (Figure 2B). The 153rd amino acid is located in the death domain of EDARADD and is highly conserved in vertebrates (Figure 2C). These findings suggest that the Pro153Ser missense mutation of the *Edaradd* gene is causative of the phenotypes of *swh/swh* rats.

Reporter assay for the Pro153Ser mutant EDARADD

Overexpression of *Edaradd* in 293T cells activates NF-κB in a dose-dependent manner [25]. To examine whether Pro153Ser *Edaradd* can activate NF-κB, we carried out a reporter assay. As shown in Figure 3, wild-type *Edaradd*

Table 1 PCR primers used to amplify rat *Edaradd* cDNA

Primer set	Forward (5' > 3')	Reverse (5' > 3')
Edaradd-1&2	CTGAGAGAGAGTCGCGCATT	GCCACAGCTGTTCCCATAG
Edaradd-3&4	GCCCAGAAAAGGCAGCTC	GGAAAACCTTTGGAGTTTCTGA
Edaradd-5&6	CGATGAGCCAGCTTTACCTC	GGATAATTGGGTAACTATTCTCAACC
Edaradd-7&8	TCCATCCCAATTTTACCAACA	CGGCAAGCATTTTAATGACC
Edaradd-9&10	CAGTCAGCCCCTTGCACT	GCATGCTCTCATCAACATGG
Edaradd-11&12	TGTCACCAATGTGGTAGAAAAA	CAGGGATAACCACTGCCTGT

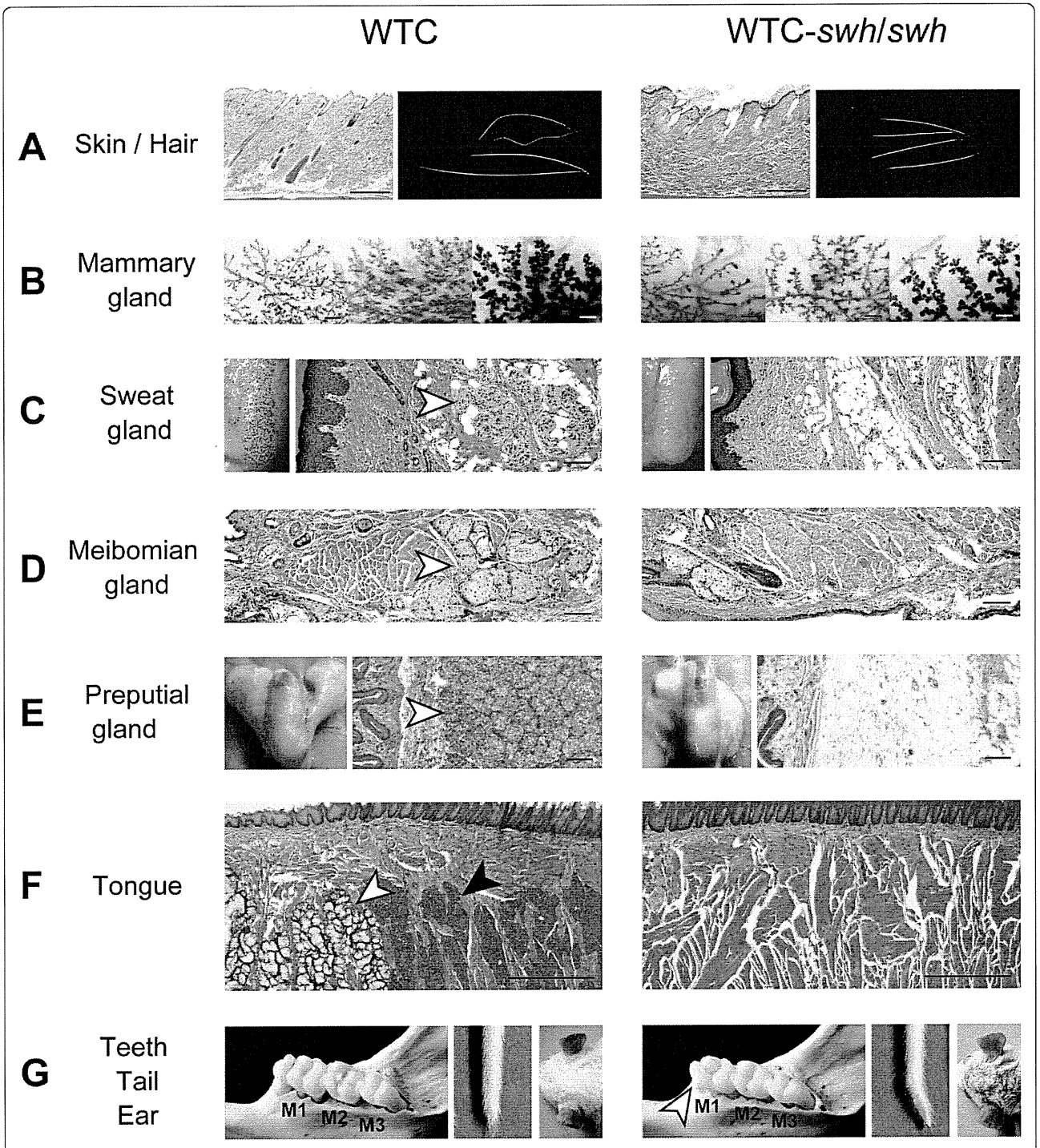

Figure 1 Phenotypes of the swh/swh rat as hypohidrotic ectodermal dysplasia (HED). A, Sections of the dorsal skin (left) and hair (right). Incomplete hair follicles are evident in *swh/swh* rat. Scale bar, 0.5 mm. The WTC rat has four hair types; auchene, zigzag, awl and guard, while the *swh/swh* rat have only the abnormal awl hair. B, Whole mount stained mammary glands; 6-week-old (left), 8-week-old (center), and pregnant day 9 (right). Mammary gland branching is poor in *swh/swh* rat. Scale bar, 1 mm. C, Sweat test results (left) and section of the footpads. Sweat, detected as dark spots, is not seen in *swh/swh* rat. Sweat glands (arrowhead) are present in WTC rat and absent in *swh/swh* rat. Scale bar, 100 μm. D, Sections of the eyelid. The meibomian glands (arrowhead) are present in WTC rat and absent in *swh/swh* rat. Scale bar, 100 μm. E, An entire view (left) and a section of the preputial gland (right). The preputial gland is atrophied in male *swh/swh* rat. Acinous glands (arrowhead) are present in WTC rat and absent in *swh/swh* rat. Scale bar, 100 μm. F, Section of the tongue. Both mucous (open arrowhead) and serous (filled arrowhead) glands are present in WTC rat and neither is seen in *swh/swh* rat. Scale bar, 0.5 mm. **G**, Buccal views of lower molars (left), tip of tail (center), and posterior auricular region (right). Cusp number is reduced in the first molar (arrow head) in *swh/swh* rat. Some *swh/swh* rats show the kink tail. The bald patch behind the ear was not evident in the *swh/swh* rat.

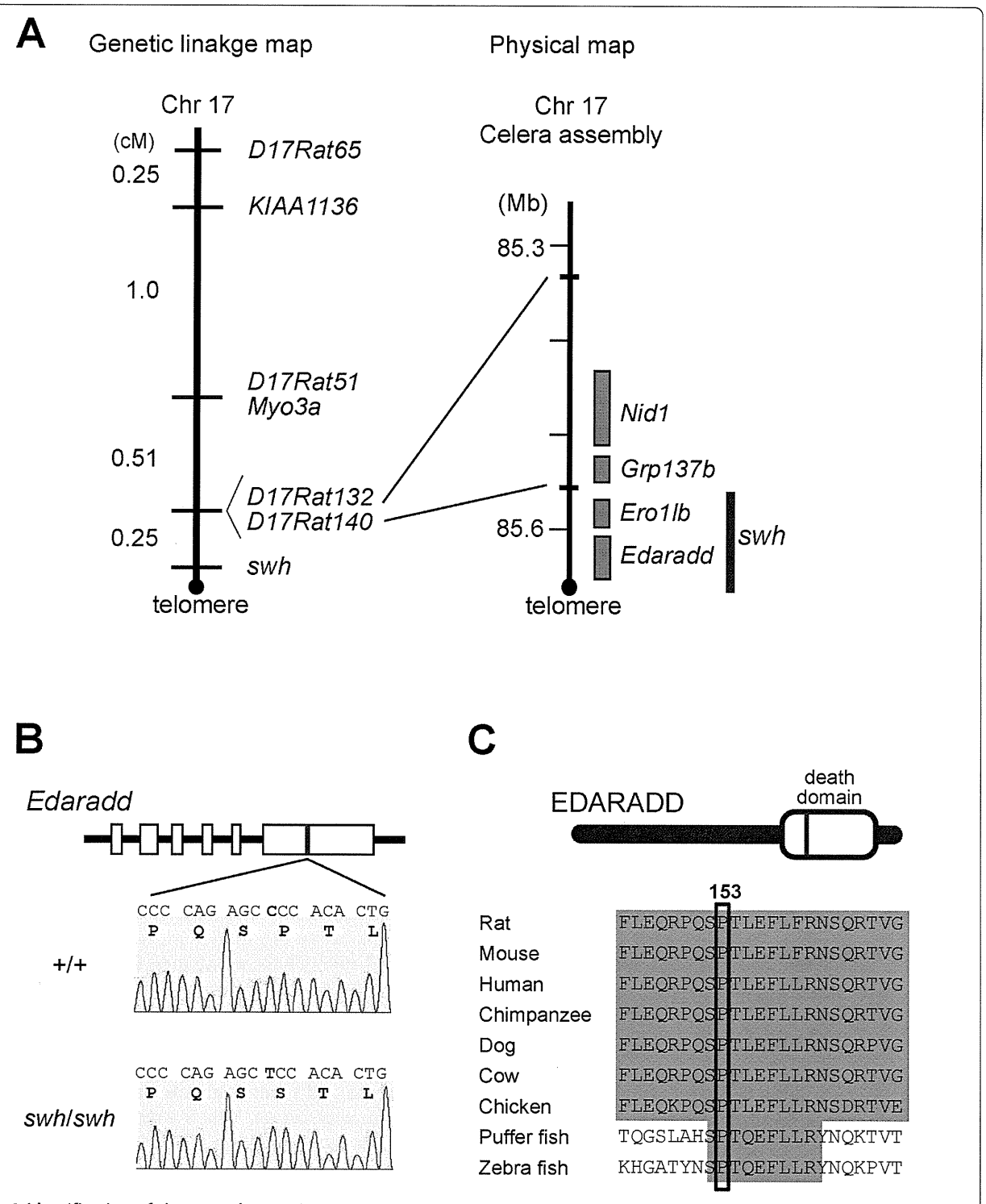

Figure 2 Identification of the rat *swh* mutation. A, Fine mapping of *swh* (left) and physical mapping of *swh* (right). The *swh* genetically mapped to the most telomeric part of rat Chr17, 0.25-cM distal from *D17Rat132* and *D17Rat140*. In the physical map, the *swh* locus is localized to a ~0.2-Mb region between *D17Rat140* and the telomere. Both *Ero1lb* and *Edaradd* have been mapped within the *swh* locus. B, Sequence analysis of *Edaradd* gene of wild-type and *swh/swh* rats. In the genomic DNA of *swh/swh* rat, a C to T (red) transition is present in exon 6 of rat *Edaradd* gene. This changes proline to serine at codon 153 of the deduced EDARADD protein. Rat codon 153 corresponds to codon 156 of mouse EDARADD isoform 1 (NP_598398) and codon 153 human EDARADD isoform B (NP_542776). C, Amino-acid sequence alignment of a region of the EDARADD death domain from different species. The 153rd amino acid that is altered in *swh/swh* rat is highly conserved in the vertebrates.

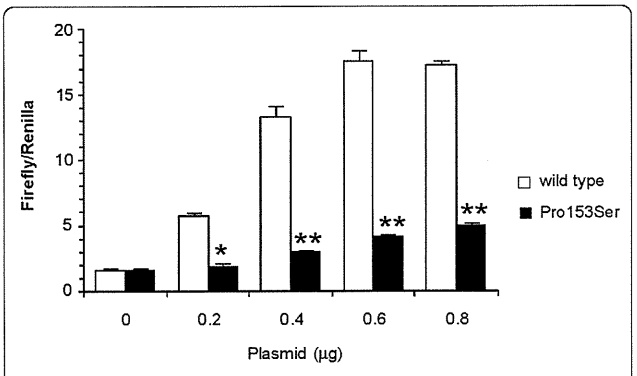

Figure 3 Loss of NF-κB activation by the Pro153Ser Edaradd mutant protein. 293T cells were transfected with 1.2 μg pNF-κB-luciferase reporter gene plasmid, 2 μg pRL-TK, and the amounts of each expression construct were measured in a reporter assay. The expression levels of luciferase were normalized to those of the internal control. Relative NF-κB activity in wild-type transfected cells increased in a dose-dependent manner, while significantly lower relative NF-κB activity was observed in the Pro153Ser *Edaradd*-transfected cells. *P < 0.01, **P < 0.001.

activated NF-κB in a dose-dependent manner. Meanwhile, Pro153Ser *Edaradd* showed significantly lower transcriptional activity of NF-κB than the wild type. The expression level of the Pro153Ser EDARADD protein detected by western blotting was not different from that of the wild type (data not shown). These findings indicate that the Pro153Ser missense mutation of the rat *Edaradd* gene could not activate NF-κB and that the Eda signaling pathway failed to function in *swh/swh* rats.

Discussion

In this study, we demonstrated that the *swh/swh* rat harbored a Pro153Ser mutation in the *Edaradd* gene and showed typical symptoms of HED, such as sparse hair, oligodontia, inability to sweat, and developmental defects of the ectoderm-derived glands [27]. Hence, we successfully established the *swh/swh* rat as a genetically and phenotypically well-characterized disease model of HED.

EDARADD is a 208 amino acid protein consisting of an N-terminal Tnf receptor-associated factor (Traf)-binding consensus sequence and a C-terminal death domain (DD). The Traf-binding consensus sequence of EDARADD is used as a docking site for Traf1, Traf2, and Traf3, thereby recruiting Traf members and leading eventually to the activation of NF-κB [6]. The DD is involved in self-association of EDARADD and its interaction with EDAR [6,25]. Thus, EDARADD is central to Edar signaling. The N-terminal region is responsible for signal transduction and the C-terminal DD is required for receptor engagement.

To date, four *EDARADD* mutations have been found in a subset of human HED, one leads to autosomal dominant inheritance (Leu112Arg) [26], while the others lead to autosomal recessive inheritance (Glu142Lys, Pro121Ser, and Thr135-Val136del) [6,28,29]. All of these mutations are located in the DD and functional analyses showed that they resulted in the failure of EDARADD to interact with EDAR and to activate NF-κB. In the *crinkled* mouse, a genomic region of ~66-kb or more which includes exon 6 that encodes the entire DD, is deleted [25]. The *crinkled* mouse displays developmental defects in hair follicles, teeth, and sweat glands [30,31]. Hence, it is possible that a mutation in the DD of EDARADD is necessary for the HED syndrome to be manifested both in human and mouse.

All members of the DD superfamily form a highly compact structure comprising six antiparallel α-helix that is involved in homotypic and heterotypic protein-protein complex formation [32]. The region spanning the α1 to α4 helices of the DD of MyD88, a member of the death receptor superfamily, is required for its interaction with a downstream kinase [33]. A comparison of the amino acid sequences of the DD superfamily revealed that the Pro153-Ser missense mutation found in the present study is located in the α4 helix of the DD of EDARADD. This mutation may cause a profound change in the polarity of a crucial region and eventually diminish NF-κB signaling. It is likely that Pro153Ser affects the structure of the DD thereby interfering in the interaction of EDARADD with EDAR.

Mutations affecting the Eda pathway are known in medaka [13], zebrafish [14], mouse [4,6,8], cattle [15-18], dog [19], and human [3,5,6]. Of them, the mouse mutants have been widely characterized as a model organism of HED. Here we report the *swh* mutation as the first example of a mutation in the Eda pathway in the rat.

Because the rat is closely related to the mouse, it is important to recognize how the rat *Edaradd* mutant phenotype matches the mouse Eda pathway mutant phenotypes. Similar to the mouse mutants, the *swh/swh* rat displayed sparse hair, misshapen teeth, and absence of sweating. Additionally, like the Eda pathway mutant, the *swh/swh* rat had only abnormal awl hair in the coat. The *swh/swh* rat showed a lack of the ectoderm-derived glands, meibomian, preputial, and tongue. Interestingly, both serous and mucous glands were absent in the tongue of the *swh/swh* rat. This is a clear difference from the mouse Eda pathway mutants that lacked mucous glands but had serous glands in the tongue [34]. Moreover, in contrast to the complete absence of tail hair in the Eda pathway mutant mice, the *swh/swh* rat had hair on its tail. The penetrance of the kink tail phenotype was low in the *swh/swh* rat, while almost all Eda pathway mutant mice showed the kink tail. Lastly, the bald patch behind the ear was not present in the *swh/swh* rat, although it was a very characteristic phenotype of the Eda pathway mutant mice.

Why these phenotypes are different between the Eda pathway mutant mice and the *swh/swh* rats is yet to be explained. However, different types of mutations could possibly explain the differences. The mouse *crinkled* mutation is a deletion [6], while the *swh* mutation is missense. Although the Luc-reporter assay strongly suggested that *swh* is a null mutation, the possibility that *swh* might be a hypomorphic mutation cannot be eliminated because the activation of NF-κB found in the assay was very low. In the Eda pathway mutant mice, the mammary, salivary and tracheal submucosal glands have been well characterized [9,10]. Further analyses of these glands in *swh/swh* rats will give further insights into the functions of the Eda pathway genes in the development of these glands.

Conclusions

We successfully established the *swh/swh* rat as the first rat model of HED and identified *swh* as a Pro135Ser missense mutation in the *Edaradd* gene. The Pro135Ser mutant protein failed to activate NF-κB in the Eda signaling pathway. Thus, the *swh/swh* rat is a good model that can be used to investigate the pathological basis of HED.

Acknowledgements and Funding

The authors are grateful to the National BioResource Project for the Rat for providing the ACI/NKyo, WTC/Kyo, and WTC-*swh*/Kyo rat strains. This work was supported in part by the Grants-in-aid for Scientific Research from the Japan Society for the Promotion of Science (21300153 to TK) and by a Grant-in-aid for Cancer Research from the Ministry of Health, Labour and Welfare (to TK).

Authors' contributions

TK and MY performed the genetic and molecular biological experiments. RH and HH performed the histological examinations. TK wrote the paper and HH and TS revised the manuscript. All authors read and approved the final manuscript.

Received: 29 July 2011 Accepted: 21 October 2011
Published: 21 October 2011

References

1. Mikkola ML, Thesleff I: **Ectodysplasin signaling in development.** *Cytokine Growth Factor Rev* 2003, **14(3-4)**:211-224.
2. Salisbury DM, Stothers JK: **Hypohidrotic ectodermal dysplasia and sudden infant death.** *Lancet* 1981, **1(8212)**:153-154.
3. Kere J, Srivastava AK, Montonen O, Zonana J, Thomas N, Ferguson B, Munoz F, Morgan D, Clarke A, Baybayan P, *et al*: **X-linked anhidrotic (hypohidrotic) ectodermal dysplasia is caused by mutation in a novel transmembrane protein.** *Nat Genet* 1996, **13(4)**:409-416.
4. Srivastava AK, Pispa J, Hartung AJ, Du Y, Ezer S, Jenks T, Shimada T, Pekkanen M, Mikkola ML, Ko MS, *et al*: **The Tabby phenotype is caused by mutation in a mouse homologue of the *EDA* gene that reveals novel mouse and human exons and encodes a protein (ectodysplasin-A) with collagenous domains.** *Proc Natl Acad Sci USA* 1997, **94(24)**:13069-13074.
5. Monreal AW, Ferguson BM, Headon DJ, Street SL, Overbeek PA, Zonana J: **Mutations in the human homologue of mouse dl cause autosomal recessive and dominant hypohidrotic ectodermal dysplasia.** *Nat Genet* 1999, **22(4)**:366-369.
6. Headon DJ, Emmal SA, Ferguson BM, Tucker AS, Justice MJ, Sharpe PT, Zonana J, Overbeek PA: **Gene defect in ectodermal dysplasia implicates a death domain adapter in development.** *Nature* 2001, **414(6866)**:913-916.
7. Mikkola ML: **Molecular aspects of hypohidrotic ectodermal dysplasia.** *Am J Med Genet A* 2009, **149A(9)**:2031-2036.
8. Headon DJ, Overbeek PA: **Involvement of a novel Tnf receptor homologue in hair follicle induction.** *Nat Genet* 1999, **22(4)**:370-374.
9. Chang SH, Jobling S, Brennan K, Headon DJ: **Enhanced Edar signalling has pleiotropic effects on craniofacial and cutaneous glands.** *PLoS One* 2009, **4(10)**:e7591.
10. Melnick M, Phair RD, Lapidot SA, Jaskoll T: **Salivary gland branching morphogenesis: a quantitative systems analysis of the Eda/Edar/NFκB paradigm.** *BMC Dev Biol* 2009, **9**:32.
11. Gruneberg H: **The glandular aspects of the tabby syndrome in the mouse.** *J Embryol Exp Morphol* 1971, **25(1)**:1-19.
12. Gaide O, Schneider P: **Permanent correction of an inherited ectodermal dysplasia with recombinant EDA.** *Nat Med* 2003, **9(5)**:614-618.
13. Kondo S, Kuwahara Y, Kondo M, Naruse K, Mitani H, Wakamatsu Y, Ozato K, Asakawa S, Shimizu N, Shima A: **The medaka *rs-3* locus required for scale development encodes ectodysplasin-A receptor.** *Curr Biol* 2001, **11(15)**:1202-1206.
14. Harris MP, Rohner N, Schwarz H, Perathoner S, Konstantinidis P, Nusslein-Volhard C: **Zebrafish eda and edar mutants reveal conserved and ancestral roles of ectodysplasin signaling in vertebrates.** *PLoS Genet* 2008, **4(10)**:e1000206.
15. Drogemuller C, Distl O, Leeb T: **Partial deletion of the bovine *ED1* gene causes anhidrotic ectodermal dysplasia in cattle.** *Genome Res* 2001, **11(10)**:1699-1705.
16. Drogemuller C, Peters M, Pohlenz J, Distl O, Leeb T: **A single point mutation within the *ED1* gene disrupts correct splicing at two different splice sites and leads to anhidrotic ectodermal dysplasia in cattle.** *J Mol Med (Berl)* 2002, **80(5)**:319-323.
17. Ogino A, Kohama N, Ishikawa S, Tomita K, Nonaka S, Shimizu K, Tanabe Y, Okawa H, Morita M: **A novel mutation of the bovine *EDA* gene associated with anhidrotic ectodermal dysplasia in Holstein cattle.** *Hereditas* 2011, **148(1)**:46-49.
18. Gargani M, Valentini A, Pariset L: **A novel point mutation within the *EDA* gene causes an exon dropping in mature RNA in Holstein Friesian cattle breed affected by X-linked anhidrotic ectodermal dysplasia.** *BMC Vet Res* 2011, **7**:35.
19. Casal ML, Scheidt JL, Rhodes JL, Henthorn PS, Werner P: **Mutation identification in a canine model of X-linked ectodermal dysplasia.** *Mamm Genome* 2005, **16(7)**:524-531.
20. Kuramoto T, Morimura K, Nomoto T, Namiki C, Hamada S, Fukushima S, Sugimura T, Serikawa T, Ushijima T: **Sparse and wavy hair: a new model for hypoplasia of hair follicle and mammary glands on rat chromosome 17.** *J Hered* 2005, **96(4)**:339-345.
21. Saar K, Beck A, Bihoreau MT, Birney E, Brocklebank D, Chen Y, Cuppen E, Demonchy S, Dopazo J, Flicek P, *et al*: **SNP and haplotype mapping for genetic analysis in the rat.** *Nat Genet* 2008, **40(5)**:560-566.
22. Rothschild TC, Boylan ES, Calhoon RE, Vonderhaar BK: **Transplacental effects of diethylstilbestrol on mammary development and tumorigenesis in female ACI rats.** *Cancer Res* 1987, **47(16)**:4508-4516.
23. Kuramoto T, Kuwamura M, Tokuda S, Izawa T, Nakane Y, Kitada K, Akao M, Guenet JL, Serikawa T: **A mutation in the gene encoding mitochondrial Mg^{2+} channel MRS2 results in demyelination in the rat.** *PLoS Genet* 2011, **7(1)**:e1001262.
24. Reed WB, Lopez DA, Landing B: **Clinical spectrum of anhidrotic ectodermal dysplasia.** *Arch Dermatol* 1970, **102(2)**:134-143.
25. Yan M, Zhang Z, Brady JR, Schilbach S, Fairbrother WJ, Dixit VM: **Identification of a novel death domain-containing adaptor molecule for ectodysplasin-A receptor that is mutated in crinkled mice.** *Curr Biol* 2002, **12(5)**:409-413.
26. Bal E, Baala L, Cluzeau C, El Kerch F, Ouldim K, Hadj-Rabia S, Bodemer C, Munnich A, Courtois G, Sefiani A, *et al*: **Autosomal dominant anhidrotic ectodermal dysplasias at the EDARADD locus.** *Hum Mutat* 2007, **28(7)**:703-709.
27. Pispa J, Thesleff I: **Mechanisms of ectodermal organogenesis.** *Dev Biol* 2003, **262(2)**:195-205.
28. Chassaing N, Cluzeau C, Bal E, Guigue P, Vincent MC, Viot G, Ginisty D, Munnich A, Smahi A, Calvas P: **Mutations in *EDARADD* account for a small proportion of hypohidrotic ectodermal dysplasia cases.** *Br J Dermatol* 2010, **162(5)**:1044-1048.
29. Suda N, Bazar A, Bold O, Jigjid B, Garidkhuu A, Ganburged G, Moriyama K: **A Mongolian patient with hypohidrotic ectodermal dysplasia with a novel P121S variant in *EDARADD*.** *Orthod Craniofac Res* 2010, **13(2)**:114-117.

30. Kindred B: **The expression of the Tabby and crinkled genes in different genetic backgrounds in the mouse.** *Genetics* 1967, **55(1)**:173-178.
31. Rao MS, Jaszczak E, Landis SC: **Innervation of footpads of normal and mutant mice lacking sweat glands.** *J Comp Neurol* 1994, **346(4)**:613-625.
32. Weber CH, Vincenz C: **The death domain superfamily: a tale of two interfaces?** *Trends Biochem Sci* 2001, **26(8)**:475-481.
33. Loiarro M, Gallo G, Fanto N, De Santis R, Carminati P, Ruggiero V, Sette C: **Identification of critical residues of the MyD88 death domain involved in the recruitment of downstream kinases.** *J Biol Chem* 2009, **284(41)**:28093-28103.
34. Wells KL, Mou C, Headon DJ, Tucker AS: **Defects and rescue of the minor salivary glands in Eda pathway mutants.** *Dev Biol* 2011, **349(2)**:137-146.

doi:10.1186/1471-2156-12-91
Cite this article as: Kuramoto *et al.*: A rat model of hypohidrotic ectodermal dysplasia carries a missense mutation in the *Edaradd* gene. *BMC Genetics* 2011 **12**:91.

Brain Research Bulletin 86 (2011) 36–41

Contents lists available at ScienceDirect

Brain Research Bulletin

journal homepage: www.elsevier.com/locate/brainresbull

Research report

Neuroprotective effect of levetiracetam on hippocampal sclerosis-like change in spontaneously epileptic rats

Sei Sugata[a], Ryosuke Hanaya[a,*], Kenta Kumafuji[b], Mai Tokudome[a], Tadao Serikawa[b], Kaoru Kurisu[c], Kazunori Arita[a], Masashi Sasa[d]

[a] Department of Neurosurgery, Graduate School of Medical and Dental Sciences, Kagoshima University, Kagoshima 890-8544, Japan
[b] Institute of Laboratory Animals, Graduate School of Medicine, Kyoto University, Kyoto 606-8501, Japan
[c] Department of Neurosurgery, Graduate School of Biomedical Sciences, Hiroshima University, Hiroshima 734-8551, Japan
[d] Nagisa Clinic, Hirakata 573-1183, Japan

ARTICLE INFO

Article history:
Received 6 April 2011
Received in revised form 16 May 2011
Accepted 30 May 2011
Available online 6 June 2011

Keywords:
Levetiracetam
Neuroprotection
Spontaneous epileptic rat (SER)
Hippocampal cell loss
Mossy fiber sprouting
Brain-derived neurotrophic factor (BDNF)

ABSTRACT

The spontaneously epileptic rat (SER) begins to exhibit both tonic convulsions and absence seizures from 6 weeks of age and SERs have stable seizures after 10 weeks of age. Low-dose administrations of levetiracetam (LEV) for 4- to 5-weeks-old SERs which did not show spontaneous seizures reduced both seizures 5 weeks after termination of administration. The hippocampus of SER exhibited decreased CA3 neurons, sprouting of mossy fibers, and hyperexpression of the brain-derived neurotrophic factor (BDNF). We attempted prophylactic LEV administrations in preseizure-manifesting SERs to evaluate if such a treatment regimen would protect the hippocampal sclerosis-like changes observed in SERs. The osmotic mini-pump administered LEV dissolved in saline to 4-weeks-old SERs for 4 weeks at 2.5 μl/h. LEV was administered at 420 mg/ml for 4 weeks in Group A. In Group B, LEV was given at 420 mg/ml for the first 2 weeks followed by doubling the dosage (840 mg/ml) in the following 2 weeks. LEV administrations in preseizure-manifesting SERs reduced the decrease of CA3 neurons and mossy fibers sprouting at 10–11 weeks of age in both group A and B. LEV attenuated BDNF expression in inner molecular layers of the dentate gyrus, striatum radiatum, and CA3 in 10- to 11- and 14- to 15-weeks-old SERs. In group B, LEV decreased BDNF expression in hilus and CA1 of 10- to 11- weeks-old SER. The present results suggest that prophylactic treatment with LEV in preseizure-manifesting SERs inhibits hippocampal sclerosis-like neuronal degeneration and/or regeneration.

1. Introduction

Levetiracetam (LEV) is a pyrrolidone derivative structurally related to piracetam [6], and the chemical structure is different from other currently available antiepileptic agents. LEV is extensively used for partial and/or generalized epilepsy since 2002 [17,24]. LEV shows a unique, antiepileptic profile and recent findings have revealed that LEV binds to SV2A protein, which presumably is involved in regulating neurotransmitter release [28]. During the process of epileptogenesis, manifestations of certain characteristic histological changes, including neuronal death/loss and neurogenesis leading to reorganization of cell membrane matrixes and formation of axonal/dendritic sprouting and gliosis, are obvious [34]. In fact, cellular network alterations composed of neuronal loss, axonal sprouting, gliosis and reorganization of neuronal circuits have been demonstrated [21,47]. However, there are some reports showing that LEV may have a neuroprotective effect against epileptogenesis: LEV exhibits neuroprotective effects on kinic acid-induced toxicity [30] and stroke and head injuries in an experimental model [11,43].

Thus, in an attempt to elucidate whether LEV elicited an antiepileptogenic activity, the effects of LEV on neuronal loss, sprouting and brain derived neurotrophic factor (BDNF) expression were examined using SERs in this study. The SER (*zi/zi, tm/tm*) is a double mutant obtained by mating heterozygous tremor rats (*tm/+*), a mutant found in an inbred colony of Kyoto-Wistar rats [44], with homozygous zitter rats (*zi/zi*) found in a Sprague-Dawley colony [36]. SERs at 6 weeks (wk) of age begin to spontaneously show tonic convulsion and absence seizures. The seizures increase in accordance with aging, and frequency and duration of the seizures did not have age-related differences in SER after 10 wk of age [40]. Each seizure was characterized by low voltage fast waves and 5–7 Hz spike-wave-like seizures in cortical and hippocampal EEG, respectively [37,39]. The antiepileptic profiles of conventional antiepileptic drugs on SER parallel those in human epilepsy [37]. We

* Corresponding author at: Department of Neurosurgery, Graduate School of Medical and Dental Sciences, Kagoshima University, 8-35-1 Sakuragaoka, Kagoshima 890-8544, Japan. Tel.: +81 99 275 5375; fax: +81 99 265 4041.
E-mail address: hanaya@m2.kufm.kagoshima-u.ac.jp (R. Hanaya).

0361-9230/$ – see front matter © 2011 Elsevier Inc. All rights reserved.
doi:10.1016/j.brainresbull.2011.05.017